Journal of ELECTRONIC MATERIALS, Vol. 46, No. 1, 2017
DOI: 10.1007/s11664-016-4864-z
© 2016 The Minerals, Metals & Materials Society

Electronic, Mechanical, and Dielectric Properties of Two-Dimensional Atomic Layers of Noble Metals

POOJA KAPOOR,[1,5] JAGDISH KUMAR,[2] ARUN KUMAR,[3] ASHOK KUMAR,[4] and P.K. AHLUWALIA[1,6]

1.—Physics Department, Himachal Pradesh University, Shimla, Himachal Pradesh 171005, India. 2.—Physics Department, Central University of Himachal Pradesh, Dharamshala, Himachal Pradesh, India. 3.—Physics Department, Govt. College Banjar, Kullu, Himachal Pradesh, India. 4.—Centre for Physical Sciences, School of Basic and Applied Sciences, Central University of Punjab, Bathinda 151001, India. 5.—e-mail: pupooja16@gmail.com. 6.—e-mail: pk_ahluwalia7@yahoo.com

We present density functional theory-based electronic, mechanical, and dielectric properties of monolayers and bilayers of noble metals (Au, Ag, Cu, and Pt) taken with graphene-like hexagonal structure. The Au, Ag, and Pt bilayers stabilize in AA-stacked configuration, while the Cu bilayer favors the AB stacking pattern. The quantum ballistic conductance of the noble-metal mono- and bilayers is remarkably increased compared with their bulk counterparts. Among the studied systems, the tensile strength is found to be highest for the Pt monolayer and bilayer. The noble metals in mono- and bilayer form show distinctly different electron energy loss spectra and reflectance spectra due to the quantum confinement effect on going from bulk to the monolayer limit. Such tunability of the electronic and dielectric properties of noble metals by reducing the degrees of freedom of electrons offers promise for their use in nanoelectronics and optoelectronics applications.

Key words: Density functional theory (DFT), electronic properties, mechanical properties, dielectric properties, noble-metal atomic layers

INTRODUCTION

Noble metals in the form of nanoparticles,[1] nanowires, nanorods, nanoclusters,[2] and nanosheets have attracted immense interest due to their encouraging applications in the fields of electronics,[2] catalysis, photonics, and sensing.[3,4] In the past, special attention has been paid to shape- and size-controlled synthesis of noble-metal nanoparticles due to their wide range of tunable properties[5–8] for application in nano-biosensing,[9] surface-enhanced Raman spectroscopy (SERS),[10,11] diagnostics,[12] photothermal and therapeutic applications,[13] generation of nanophotonic devices,[14] and related biological and medical fields.[15,16] The optical properties of metallic (Ag, Cu) nanoparticles (NPs) embedded in glass matrices have received huge attention from the viewpoints of basic research and their applications.[17,18]

Noble metals in two-dimensional (2D) form with thickness ranging from 10 nm to 500 nm possess unusual physical[19] and chemical properties[20] due to strong quantum confinement and surface effects. Two-dimensional layers of noble metals have numerous technological applications, e.g., in catalysis,[21,22] microelectromechanical and nanoelectromechanical systems, as interconnects in molecular circuits, sensors,[23] plasmonics,[24] devices for surface-enhanced Raman spectroscopy (SERS),[25] and the biomedical area.[26] Furthermore, it is expected that various new materials in the form of nanoclusters, nanorods, nanoflakes, nanoribbons, and nanocages can be derived by using these nanolayers as building blocks.[27]

(Received March 24, 2016; accepted August 8, 2016; published online August 22, 2016)

Recently, experiments using gold nanolayers were carried out, revealing promising applications in next-generation electronic devices.[28–33] Au multilayers have been used as stretchable electrodes for organic-based electronic devices,[34] displays,[35] field-effect transistors (FETs),[36] and energy-related devices.[37] Similarly, experimentally synthesized silver nanosheets[38] have been found to be useful for tuning surface-enhanced Raman spectroscopy (SERS), metal-enhanced fluorescence, and as scanning tunneling microscopy (STM) substrates.[6] Additionally, layered Pt sheets show promise for electrochemical conversion and catalysis.[39] A 2D Cu nanosheet has also been used as a novel material for aqueous conductive ink in flexible electronics because of its low price and high conductivity.[40] Note that synthesis of Cu monolayers is challenging, with only a few techniques being available, because Cu readily converts to CuO or CuS layers.

Motivated by the above experimental results involving 2D noble-metal layers, we present herein a density functional theory (DFT)-based computational study of structural, electronic, mechanical, and dielectric properties of monolayers and bilayers of noble metals (Cu, Ag, Au, and Pt). Efforts were made to explore the structural and mechanical stability of the mono- and bilayer noble metals and the possible technological implications.

COMPUTATIONAL METHODS

All calculations were performed using the *Spanish Initiative for Electronic Simulation with Thousands of Atoms* (SIESTA) code,[41] which uses *ab initio* pseudopotential-based density functional theory (DFT). We used well-tested[42] Troullier–Martins, norm-conserving relativistic pseudopotentials[43,44] for the different noble metals in fully separable Kleinman–Bylander form. The exchange and correlation energies were treated within the generalized gradient approximation (GGA) according to the Perdew–Burke–Ernzerhof (PBE) parameterization.[45] Numerical atomic orbitals (NAOs) with a double zeta polarization (DZP) basis set with confinement energy of 0.01 Ry were used for geometry optimization. Energy minimization in each case was carried out using the standard conjugate-gradients (CG) technique. All structures were relaxed until the force on each atom was less than 0.01 eV/Å. A $40 \times 40 \times 1$ Monkhorst–Pack[46] **k**-point grid was used for sampling the Brillouin zone. The mesh cutoff energy was taken as 200 Ry. We took two atoms in the unit cell for monolayers and four atoms in the unit cell for bilayers in our calculations. A vacuum region of about 16 Å was used to separate the two-dimensional layers along the *c*-axis to ensure that there was no interaction between periodic images. Dielectric properties were

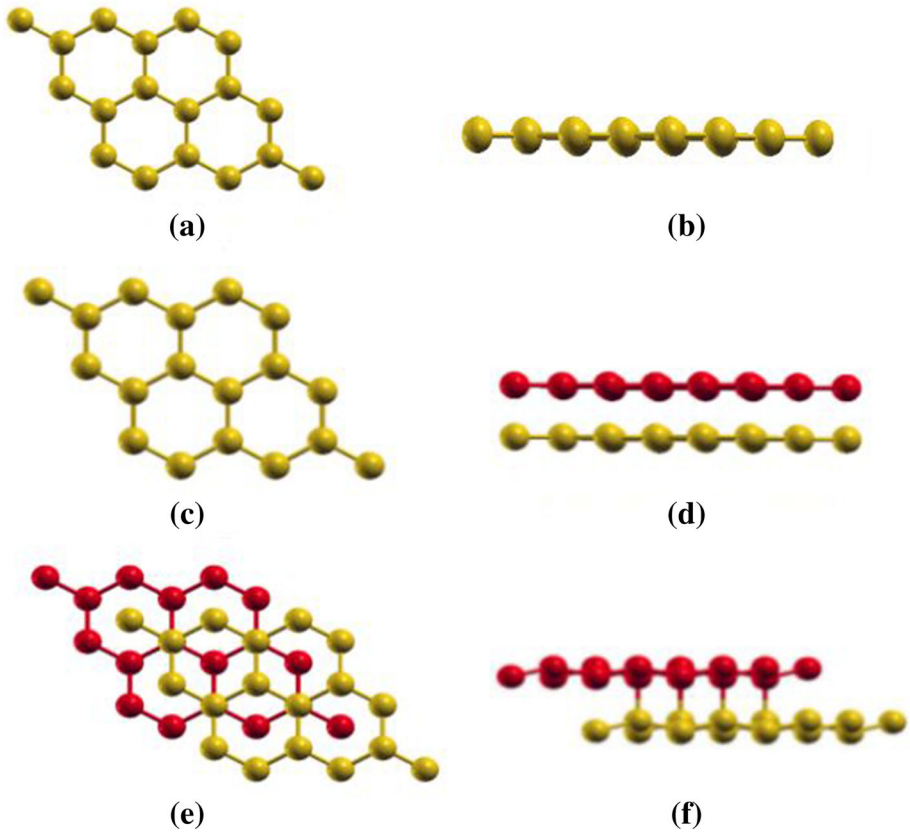

Fig. 1. (a) Top view of monolayer. (b) Side view of monolayer. (c) Top view of AA-stacked bilayer. (d) Side view of AA-stacked bilayer. (e) Top view of AB-stacked bilayer. (f) Side view of AB-stacked bilayer.

calculated using first-order time-dependent perturbation theory as implemented in the SIESTA package.[47,48] A 60 × 60 × 3 optical mesh and 0.2 eV optical broadening were used for calculations of dielectric properties. It is necessary to include a Drude term associated with intraband transitions in the case of metals, which is of the form

$$\varepsilon_{\mathrm{Drude}}(\omega) = \omega_{\mathrm{p}}^2/\omega(\omega + \mathrm{i} \times \gamma), \qquad (1)$$

where ω_{p}^2 is calculated by the SIESTA code itself and γ is an empirical parameter, which is the inverse of the relaxation time (τ). The values of γ for Cu, Ag, Au, and Pt were taken as 0.001 Ha (0.0272 eV), 0.0005 Ha (0.0136 eV), 0.003 Ha (0.0686 eV), and 0.001 Ha (0.0272 eV), respectively,[49] for bulk, monolayers, and bilayers.

RESULTS AND DISCUSSION

Since gold nanosheets (about 16 atomic layers thick) have been reported experimentally to be synthesized with hexagonal closed-packed (hcp) structure,[4] the noble-metal mono- and bilayers

Table I. Calculated values of lattice parameter (a in Å), binding energy (ΔE_{b} in eV, all values negative but minus sign omitted) for bilayers, interlayer spacing (Δd in Å), and covalency metric (C_{d} in eV)

Property	System	Cu	Ag	Au	Pt
a (Å)	Bulk	3.69 (3.62)[a]	4.19 (4.09)[a]	4.20 (4.08)[a]	4.03 (3.93)[a]
	Monolayer	4.05	4.71	4.61	4.31
	Bilayer	4.17	4.73	4.69	4.43
ΔE_{b} (eV)	Bilayer	0.59	0.47	0.40	1.31
Δd (Å)	Bilayer	2.83	2.79	2.45	2.55
C_{d} (eV)	Monolayer	−1.90	−0.77	−2.00	−2.28
	Bilayer	−1.56	−0.75	−1.69	−1.56

[a]Ref. 42.

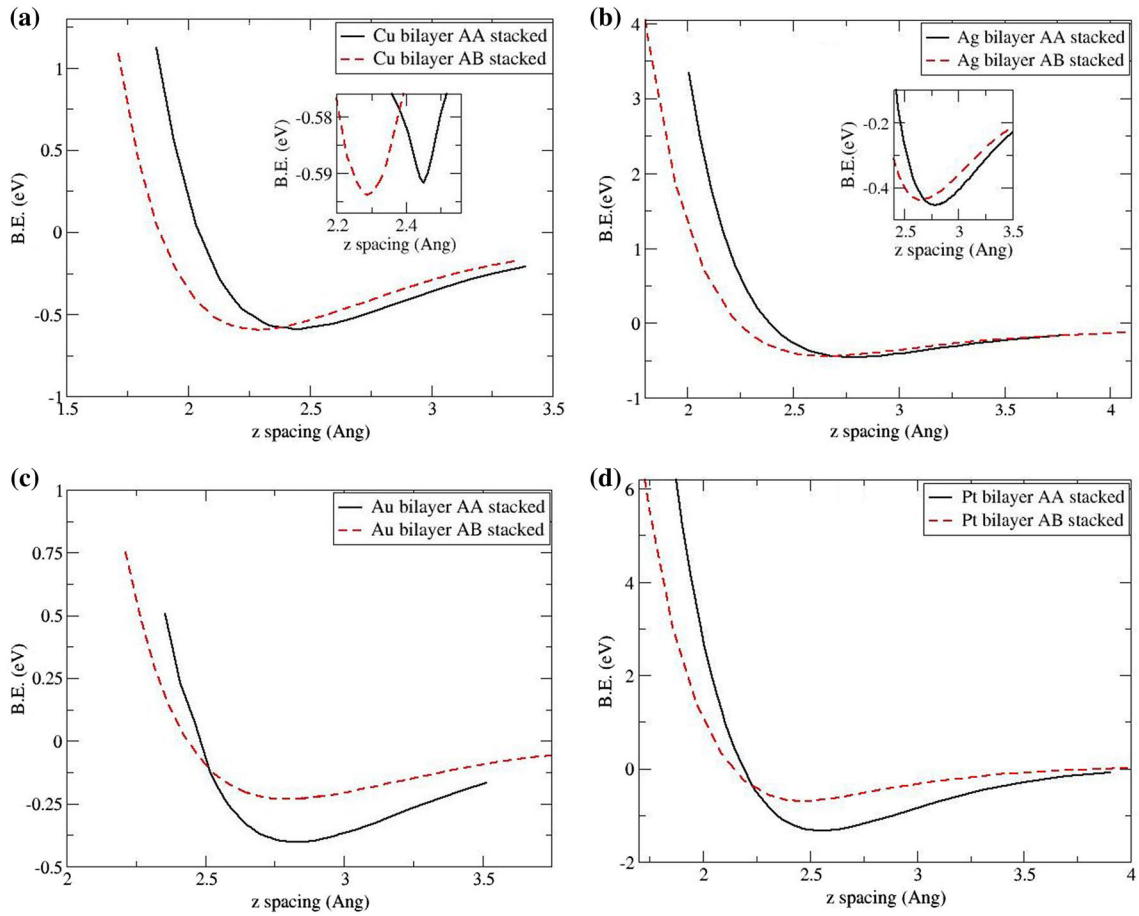

Fig. 2. Binding energy (eV) versus interlayer spacing (Å) curves for both AA- and AB-stacked bilayers of (a) Cu, (b) Ag, (c) Au, and (d) Pt.

considered here were taken with graphene-like hexagonal structure, as hcp is similar to a graphene-like structure in 2D (Fig. 1). The crystal structure taken for bulk phase was face-centered cubic (fcc), as the studied noble metals stabilize in fcc structure in bulk phase. Our calculated lattice parameters (Table I) for the bulk noble metals (Cu, Ag, Au, and Pt) (fcc structure) are consistent with values reported in literature.[49,50] The lattice constants of the graphene-like hexagonal mono- and bilayers calculated at GGA-PBE level of theory were found to be almost constant (Table I).

Being similar to a graphene-like structure, the noble-metal bilayers can have two types of stacking pattern, namely AA and AB. In AA stacking, the metal atoms of the second layer lie exactly above the noble-metal atoms of the first layer, while in the case of AB stacking, the metal atoms of the second layer lie above interstitial sites of the first layer (Fig. 1). The relative stability of the bilayers in comparison with monolayers can be seen by calculating the binding energy of the bilayers according to the formula

$$\Delta E_b = E_{bilayer} - 2E_{monolayer}, \quad (2)$$

where $E_{bilayer}$ and $E_{monolayer}$ are the minimum values of total energy of the bilayer and monolayer, respectively, obtained from total energy versus lattice constant plots. All values of ΔE_b are negative here, but we compare their magnitude only.

The curves of binding energy versus interlayer spacing suggest that Ag, Au, and Pt bilayers energetically favor AA stacking, while the Cu bilayer energetically prefers AB stacking (Fig. 2). The optimized vertical spacing between the layers was calculated to be 2.83 Å, 2.79 Å, 2.45 Å, and 2.55 Å for Cu, Ag, Au, and Pt, respectively (Table I). The calculated interlayer binding energies for the bilayers followed the order Pt > Cu > Ag > Au. The highest binding energy for the Pt bilayer is attributed to the partially filled both *s*- and *d*-orbitals.

To gain further insight into the interlayer interactions in the noble-metal bilayers, we calculated the charge density difference profiles (see Fig. S1 in the Supplementary Information; all charge density plots are at the same isosurface value of 0.0004 e/Å^3). Note that the charge density difference is defined as $\Delta\rho = \rho_{total} - (\rho_{layer1} + \rho_{layer2})$. Red regions

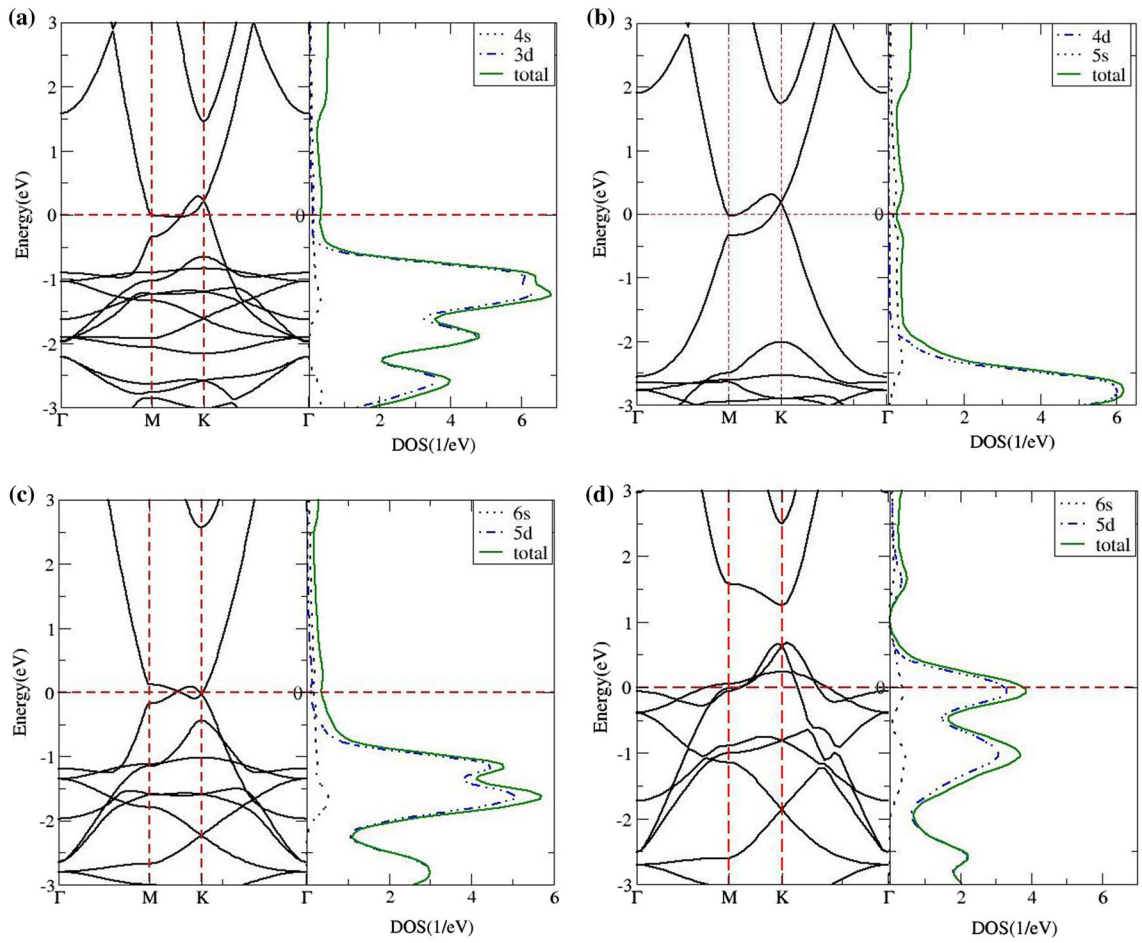

Fig. 3. Electronic band structure and corresponding density of states for monolayers of (a) Cu, (b) Ag, (c) Au, and (d) Pt. The Fermi level is set at 0 eV.

represent charge depletion, while green regions represent charge accumulation. The charge density difference plot indicates the redistribution of charge between the bonding regions of the two layers, which is more pronounced for Pt. The charge redistribution correlates well with the predicted order of interlayer binding energy, i.e., Pt > Cu > Ag > Au.

To further measure the covalent character of the bonds between atoms of the noble-metal layers, the covalency metric was calculated for all the systems and is given in Table I. The higher the value of the covalency metric, the more covalent the bond; for lower covalency, the charge distribution is enhanced. Further information and description of the concept of the covalency metric is given in the Supplementary Information and in Refs. 51 and 52. Density-of-states plots for all the systems, used to calculate the covalency, are also given in Fig. S2 in the Supplementary Information. The value of the covalency metric varied as follows: Ag > Cu > Au > Pt. This correlates well with our charge density difference plots, where charge redistribution was more pronounced for the Pt layers, which are less covalent. Also, the Ag layers, which are more covalent, have less pronounced charge redistribution. It is inferred that the bilayers are more covalent in nature than the monolayers, except in the case of Ag.

Electronic Properties

The electronic band structure of the Cu, Ag, and Au mono- and bilayers showed similar behavior, while Pt was distinctly different (Figs. 3a–d and 4a–d). The graphene-like hexagonal monolayers of Cu, Ag, and Au showed increased quantum ballistic conductance (as obtained from the number of bands crossing the Fermi level) as compared with their bulk counterparts in fcc phase.

Note that the quantum ballistic conductance is calculated from the number of bands crossing the Fermi level.[53] The band structure of bulk Cu, Ag, and Au (see Fig. S4 in the Supplementary Information) shows two bands crossing the Fermi level, yielding conductance of $2G_0$, while in the corresponding monolayers, four bands cross the Fermi level, resulting in conductance of $4G_0$. The opposite

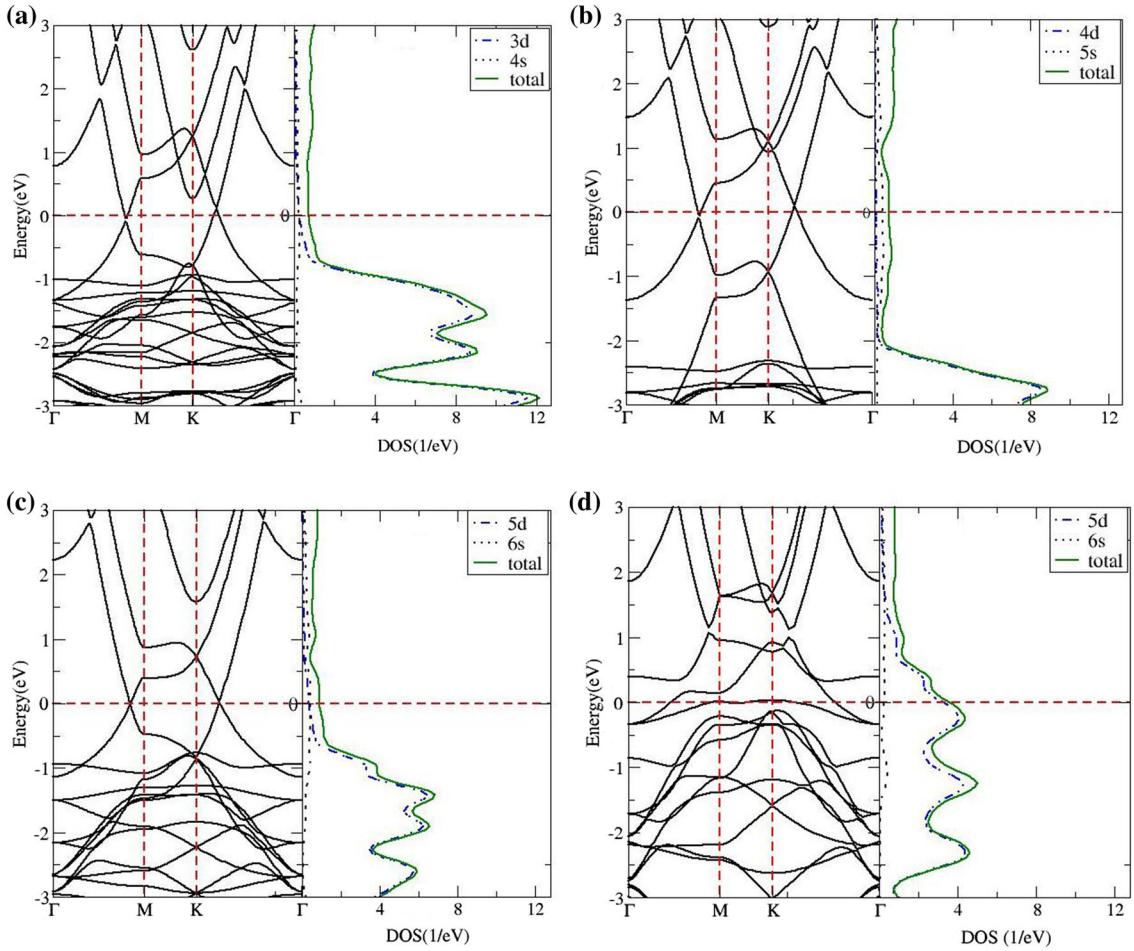

Fig. 4. Electronic band structure and corresponding density of states for bilayers of (a) Cu, (b) Ag, (c) Au, and (d) Pt. The Fermi level is set at 0 eV.

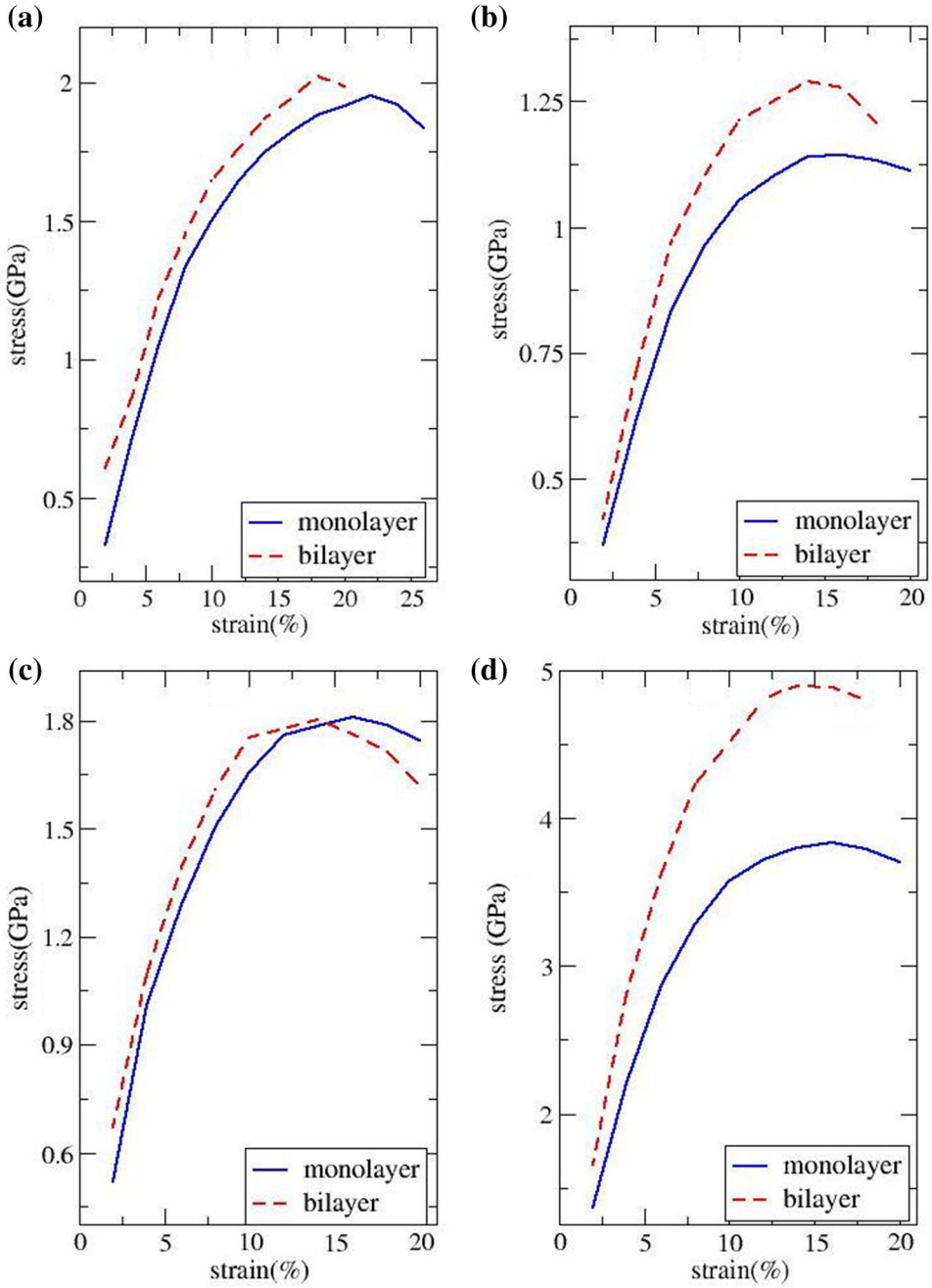

Fig. 5. Stress (GPa) versus tensile strain (%) (expansion) curve to determine the tensile strength of mono- and bilayers of (a) Cu, (b) Ag, (c) Au, and (d) Pt.

trend was observed for Pt, for which the quantum conductance decreases from $8G_0$ in bulk to $6G_0$ in the monolayer and bilayer. This is attributed to the different electronic arrangement of Pt. The value of G_0, i.e., the quantized unit of conductance, is $2e^2/h = 7.748 \times 10^{-5}$ S.

Note that, in the case of Cu, Ag, and Au, the density of states in the valence band near the Fermi level is mainly contributed by *d*-orbitals, while the conduction band near the Fermi level is mainly contributed by *s*-orbital, showing Dirac-cone-like behavior. In the case of the Pt layers, both *s*- and *d*-orbitals contribute near the Fermi level, and one observes a pronounced peak at the Fermi level, showing that the system is metallic in nature.

It is interesting to note that both the mono- and bilayers of Cu, Ag, and Au (Figs. 3 and 4) possess Dirac-cone-like (conical intersection) features. The monolayers show Dirac-cone-like behavior around the K high-symmetry point lying at the Fermi level (i.e., at 0 eV), while in the case of the bilayers, both the Γ and K high-symmetry points are found to

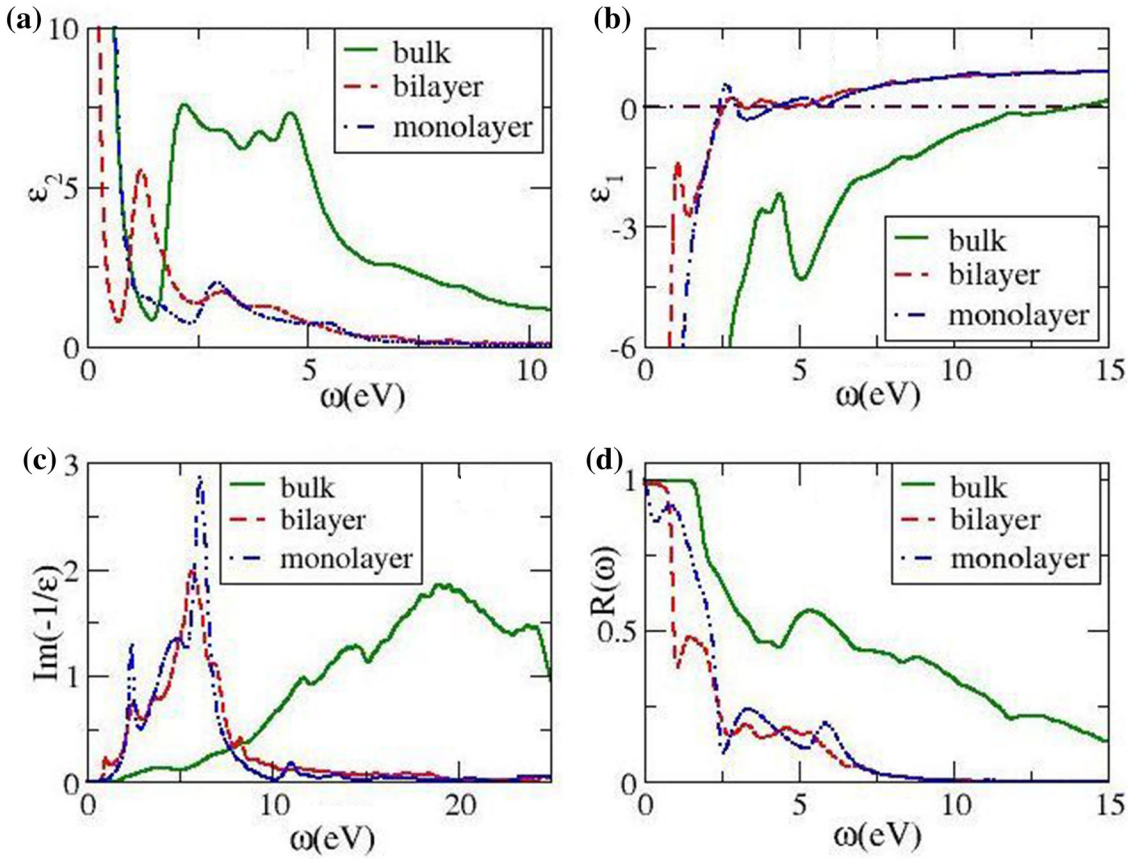

Fig. 6. (a) Imaginary part (ϵ_2) and (b) real part (ϵ_1) of dielectric function, (c) EELS spectrum, and (d) reflectance spectrum for Cu bulk, monolayer, and bilayer.

Table II. Calculated values of position of peak in ϵ_2 (S_0), plasmon frequency (ω_p), and reflectance edge [$R(\omega)$] for all studied noble-metal monolayers and bilayers and their bulk systems

Property	System	Cu	Ag	Au	Pt
S_0 (ϵ_2)	Bulk	2.23, 3.94, 4.65	3.52	2.85	6.56
	Monolayer	2.98	2.24	2.88, 4.99	1.18, 2.49, 4.403
	Bilayer	1.27	1.81	2.36, 4.98	1.072
ω_p (eV)	Bulk	11.71, 14.60, 19.02	3.09, 11.56, 22.61	2.41, 11.84, 22.42	5.90, 12.74, 23.57
	Monolayer	2.41, 6.21	3.02, 7.36	2.57, 7.53	2.16, 2.97, 5.09
	Bilayer	1.05, 2.61, 5.66	1.46, 3.36, 7.02	1.59, 2.00, 3.22, 7.45	3.38, 8.76, 10.38, 11.60
R (eV)	Bulk	1.71	2.83	1.89	5.53
	Monolayer	1.02	0.16	1.53	0.53
	Bilayer	0.73	1.32	0.75	0.11

possess the mentioned Dirac-cone-like feature, lying again at the Fermi level (i.e., at 0 eV). A recent investigation of Au/Ag multilayers using both angle-resolved photoemission spectroscopy (ARPES) and density functional theory (DFT) showed similar behavior,[54] where an anisotropic Dirac cone is observed between a particular pair of strongly spin-polarized deep *d*-orbital surface states. This interesting feature is likely to open up a new dimension for study and applications of these noble-metal mono- and bilayers.

Mechanical Properties

Mechanical strain has useful applications in nanoelectromechanical systems (NEMS) and nanooptomechanical systems (NOMS).[55] We calculated the stress that can be borne by the considered systems on application of biaxial strain. Biaxial strain was modeled by varying the lattice constant in both *a* and *b* directions. The stress varied directly with the strain up to some limit, then decreased (Fig. 5a–d). The region up to which it varied directly

is the elastic region, after which there is a plastic region, and ultimately the system deforms. The maximum value of strain up to which elasticity was retained provides the value of the ultimate tensile strain, and the corresponding stress value gives the ultimate tensile strength of the system.

The calculated ultimate tensile strength was 1.94 GPa, 1.14 GPa, 1.81 GPa, and 3.82 GPa for the Cu, Ag, Au, and Pt monolayers, respectively, while the bilayers showed slightly increased tensile strength values (Fig. 5). In the case of both monolayers and bilayers, Pt showed the highest tensile strength among the studied systems. The maximum tensile strain for the Cu mono- and bilayer was found to be 22% and 18%, respectively, while for the Ag, Au, and Pt monolayers it was 16%, and for their respective bilayers it was 14%.

The tensile strength of a material represents its capacity to withstand load or resist tension; the higher the tensile strength, the greater the capacity of a material to withstand tension. Hence, the Pt layers have higher load-withstanding capacity, followed by Cu, Au, and Ag; this trend is in agreement with the trend of tensile strength of these noble metals in bulk phase. This can be correlated with the interlayer binding energy, where greater binding energy of the system indicates stronger bonding and thus higher tensile strength.

Dielectric Properties

The calculated dielectric function for all the studied noble metal (Ag, Au, Cu, and Pt) bulks (fcc phase) agrees well with the dielectric function measured by Johnson et al.[56] and Yu et al.[57] Sharp peaks in the imaginary part of the dielectric function ϵ_2 for the studied noble metals suggest the possibility of interband transitions between bands in the band structure, corresponding to the energy values of these peaks. It was observed that peaks were red-shifted on moving from bulk in fcc phase to monolayers and bilayers taken with graphene-like hexagonal structure.

We observed sharp peaks in the imaginary part of the dielectric function ϵ_2 for bulk and bilayers of noble metals, but the monolayers showed low-valued broad peaks (except for Pt) (Figs. 6 and S5–S7 in the Supplementary Information). It was observed that the monolayer and bilayer of each of the noble metals exhibited very different ϵ_2 peak positions compared with the bulk counterparts (Table II), which may be attributed to the quantum confinement effect.[53]

Plasmon Frequency

The plasmon frequency (ω_p) corresponds to the energy (eV) at the peak in the electronic energy loss spectrum (EELS) where the curve of the real part of the dielectric function (ϵ_1) crosses the zero axis. It was found that the plasmon frequency decreased (Table II) as one goes from the bulk to the 2D limit of the noble metals Au, Ag, Cu, and Pt (Figs. 6 and S5–S7 in the Supplementary Information) due to the strong quantum confinement effect.[53]

Reflectance Spectra

The reflectance spectrum for each of the studied noble-metal mono- and bilayers showed sharp minima corresponding to the point at which ϵ_1 cuts the zero axis and EELS shows a resonance peak. The value of the energy corresponding to this minimum point gives the value of the reflectance edge (Table II). For all the studied mono- and bilayers, the reflectance edge lay in the infrared (IR) region (0 eV to 1.65 eV). The reflectance edge for bulk Cu, Ag, and Au lies in the visible region (1.65 eV to 3.22 eV), whereas for bulk Pt, it lies in the ultraviolet (UV) region (3.22 eV to 12.4 eV) (Figs. 6 and S5–S7 in the Supplementary Information). Hence, the reflectance edge of the monolayers and bilayers of the studied noble metals is red-shifted towards the infrared (IR) region compared with the bulk counterparts. Such tunability of the reflectance spectrum and dielectric function of noble metals may find interesting applications in optoelectronics.

CONCLUSIONS

Electronic, mechanical, and dielectric properties of noble-metal (Au, Ag, Cu, and Pt) mono- and bilayers with graphene-like hexagonal structure were studied, revealing significant changes on going from bulk to monolayer, summarized as follows:

- The Au, Ag, and Pt bilayers stabilized in AA-stacked configuration, while the Cu bilayer preferred AB-stacked configuration.
- The value of the covalency metric varied as Ag > Cu > Au > Pt, consistent with our charge density plots. The bilayers are more covalent than the monolayers except for Ag.
- The quantum ballistic conductance increased as one moves from bulk in fcc phase to 2D graphene-like hexagonal noble-metal monolayers and bilayers (for Ag, Au, and Cu), which may be useful in the field of nanoelectronics.
- The monolayers and bilayers of Au, Ag, and Cu exhibited a Dirac-cone-like feature, while the Pt layers were metallic in nature. The Dirac-cone-like feature obtained for the Au, Ag, and Cu atomic layers will open up new scope for their study and applications. The realization of a Dirac cone shows promise for applications of the studied noble-metal mono- and bilayers in spintronic devices and nanodevices. Further investigation of the behavior of this Dirac-cone-like feature could include functionalization of these noble-metal layers.[58]
- The Pt layers (both monolayer and bilayer) showed the highest tensile strength among the studied systems.
- The monolayers and bilayers of the studied noble metals showed distinctly different positions of

the structure peaks in ϵ_2 compared with the bulk counterparts, due to the quantum confinement effect.
- The plasmon frequency was red-shifted in energy on going from the bulk fcc structure to the graphene-like hexagonal monolayer for all the noble metals.
- The reflectance edges of the graphene-like noble-metal mono- and bilayers were found in the infrared (IR) region, in contrast to the visible–ultraviolet (UV) region for their bulk fcc counterparts, due to which they show reflectance in the infrared (IR) region and become transparent conductors in the visible region, and hence may find huge applications in optoelectronics.[49]

These atomic layers of noble metals can be used as stretchable electrodes for organic-based electronic devices,[34] displays,[35] field-effect transistors (FETs),[36] and energy-related devices,[37] as well as being useful for tuning surface-enhanced Raman spectroscopy (SERS), metal-enhanced fluorescence, and as scanning tunneling microscopy (STM) substrates.[6]

ACKNOWLEDGEMENTS

P.K. wishes to acknowledge financial support from the University Grants Commission (UGC), New Delhi in the form of a University Grants Commission Basic Sciences Research (UGC-BSR) Junior Research Fellowship (JRF). The authors would like to acknowledge the SIESTA team for the code. All calculations were carried out on the High Performance Computing Cluster (HPCC) in the Physics Department at H.P. University, provided by the Department of Science & Technology, Government of India under the Funds for the Improvement of Science & Technology (FIST) programme.

ELECTRONIC SUPPLEMENTARY MATERIAL

The online version of this article (doi: 10.1007/s11664-016-4864-z) contains supplementary material, which is available to authorized users.

REFERENCES

1. C.H. Liu, W.W. Wu, and L.J. Chen, *J. Electron. Mater.* 35, 1 (2006).
2. D.B. Janes, T. Lee, J. Liu, M. Batistuta, N.-P. Chen, B.L. Walsh, R.P. Andres, E.-H. Chen, M.R. Melloch, J.M. Woodall, and R. Reifenberger, *J. Electron. Mater.* 29, 565 (2000).
3. H.L. Liu, F. Nosheen, and X. Wang, *Chem. Soc. Rev.* 44, 3056 (2015).
4. X. Hong, C. Tan, J. Chen, Z. Xu, and H. Zhang, *Nano Res.* 8, 40 (2015).
5. D.L. Feldheim and C. Foss, *J. Am. Chem. Soc.* 124, 7874 (2002).
6. H. Chen, F. Simon, and A. Eychmuller, *J. Phys. Chem. C* 114, 4495 (2010).
7. C.J. Murphy, T.K. Sau, A.M. Gole, C.J. Orendorff, J. Gao, L. Gou, S.E. Hunyadi, and T. Li, *Phys. Chem. B* 109, 13857 (2005).
8. H.Y. Wu, H. Chu, T. Kuo, C. Kuo, and M.H. Huang, *Chem. Mater.* 17, 6447 (2005).
9. L. Lu, A. Kobayashi, K. Tawa, and Y. Ozaki, *Chem. Mater.* 18, 4894 (2006).
10. Y. Wang, X. Zou, W. Ren, W. Wang, and E. Wang, *J. Phys. Chem. C* 111, 3259 (2007).
11. A. Gentile, F. Ruffino, C. D'Andrea, P.G. Gucciardi, R. Reitano, and M.G. Grimaldi, *J. Electron. Mater.* 45, 2815 (2016).
12. L.M. Quynh, N.H. Nam, K. Kong, N.T. Nhung, I. Notingher, M. Henini, and N.H. Luong, *J. Electron. Mater.* 45, 2563 (2016).
13. S. Eustis and M.A. El-Sayed, *Chem. Soc. Rev.* 35, 209 (2006).
14. E. Ozbay, *Science* 311, 189 (2006).
15. P.K. Jain, X. Huang, I.H. El-Sayed, and M.A. El-Sayed, *Acc. Chem. Res.* 41, 1578 (2008).
16. S.E. Skrabalak, J. Chen, Y. Sun, X. Lu, L. Au, C.M. Cobley, and Y. Xia, *Acc. Chem. Res.* 41, 1587 (2008).
17. Y. Ma, J. Lin, S. Qin, L. Zhu, B. Li, and S. Lei, *J. Electron. Mater.* 41, 646 (2012).
18. J.A. Jimenez, *J. Electron. Mater.* 44, 4418 (2015).
19. A.K. Geim and K.S. Novoselov, *Nat. Mater.* 6, 183 (2007).
20. F. Geng, R. Ma, A. Nakamura, K. Akatsuka, Y. Ebina, Y. Yamauchi, N. Miyamoto, Y. Tateyama, and T. Sasaki, *Nat. Commun.* 4, 1632:1 (2013).
21. L.M. Molina and B. Hammer, *Appl. Catal.* 291, 21 (2005).
22. C. Li, W. Cai, B. Cao, F. Sun, Y. Li, C. Kan, and L. Zhang, *Adv. Funct. Mater.* 16, 83 (2006).
23. N. Krasteva, I. Besnard, B. Guse, R.E. Bauer, K. Mullen, A. Yasuda, and T. Vossmeyer, *Nano Lett.* 2, 551 (2002).
24. M.T. Do, Q.C. Tong, M.H. Luong, A. Lidiak, I.L. Rak, and N.D. Lai, *J. Electron. Mater.* 45, 2347 (2016).
25. S.-J. Hsu and I.J.B. Lin, *J. Chin. Chem. Soc.* 56, 98 (2009).
26. M.C. Daniel and D. Astruc, *Chem. Rev.* 104, 293 (2004).
27. J. Hu, Z. Wang, and J. Li, *Sensors* 7, 3299 (2007).
28. A. Sanyal and M. Sastry, *Chem. Commun.* 11, 1236 (2003).
29. S. Onoue, J. He, and T. Kunitake, *Chem. Lett.* 35, 214 (2006).
30. Z. Wang, J. Yuan, M. Zhou, L. Niu, and A. Ivaska, *Appl. Surf. Sci.* 254, 6289 (2008).
31. T.S. Selvam, C.M. Chiang, and M. Chi, *J. Nanopart. Res.* 13, 3275 (2011).
32. T. Soejima and N. Kimizuka, *Chem. Soc. Jpn.* 34, 1234 (2005).
33. X. Huang, S. Li, Y. Huang, S. Wu, X. Zhou, S. Li, C.L. Gan, F. Boey, C.A. Mirkin, and H. Zhang, *Nat. Commun.* 2, 292 (2011).
34. G.D. Moon, G.-H. Lim, J.H. Song, M. Shin, T. Yu, B. Lim, and U. Jeong, *Adv. Mater.* 25, 2707 (2013).
35. S.I. Park, Y. Xiong, R.-H. Kim, P. Elvikis, M. Meit, D.-H. Kim, J. Wu, J. Yoon, C.-J. Yu, Z. Liu, Y. Huang, K. Hwang, P. Ferreira, X. Li, K. Choquette, and J.A. Rogers, *Science* 325, 977 (2009).
36. D.-Y. Khang, H. Jiang, Y. Huang, and J.A. Rogers, *Science* 311, 208 (2006).
37. D.J. Lipomi, B.C. Tee, M. Vosgueritchian, and Z. Bao, *Adv. Mater.* 23, 1771 (2011).
38. S.H. Park, J.G. Son, T.G. Lee, H.M. Park, and J.Y. Song, *Nanoscale Res. Lett.* 8, 248 (2013).
39. A. Funatsu, H. Tateishi, K. Hatakeyama, Y. Fukunaga, T. Taniguchi, M. Koinuma, H. Matsuura, and Y. Matsumoto, *Chem. Commun.* 50, 8503 (2014).
40. R. Dang, L. Song, W. Dong, C. Li, X. Zhang, and G. Wang, *ACS Appl. Mater. Interfaces* 6, 622 (2014).
41. J.M. Soler, E. Artacho, J.D. Gale, A. Garcia, J. Junquera, P. Ordejon, and D.S. Portal, *J. Phys.: Condens. Matter* 14, 2745 (2002).
42. A. Kumar, D. Banyai, P.K. Ahluwalia, R. Pandey, and S.P. Karna, *Phys. Chem. Chem. Phys.* 16, 20157 (2014).

43. N. Troullier and J.L. Martins, *Phys. Rev. B* 43, 1993 (1991).
44. N. Troullier and J.L. Martins, *Phys. Rev. B* 43, 8861 (1991).
45. J.P. Perdew, K. Burke, and M. Ernzerhof, *Phys. Rev. Lett.* 77, 3865 (1996).
46. J. Moreno and J.M. Soler, *Phys. Rev. B* 45, 13891 (1992).
47. F. Knider, J. Hugel, and A.V. Postnikov, *J. Phys.: Condens. Matter* 19, 196105 (2007).
48. E.G. Maksimov, I.I. Mazin, S.N. Rashkeev, et al., *J. Phys. F. Met. Phys.* 18, 833 (1988).
49. A. Kumar, A. Kumar, and P.K. Ahluwalia, *Phys. E* 46, 259 (2012).
50. C. Kittel, *Introduction to Solid State Physics* (New York: Wiley Eastern Limited Reprint, 1988).
51. A. Cammarata and J.M. Rondinelli, *J. Chem. Phys.* 141, 114704 (2014).
52. A. Cammarata and T. Polcar, *Inorg. Chem.* 54, 5739 (2015).
53. B.K. Agrawal, V. Singh, R. Srivastava, and S. Agrawal, *Phys. Rev. B* 74, 245405(1) (2006).
54. R. Requist, P.M. Sheverdyaeva, P. Moras, S.K. Mahatha, C. Carbone, and E. Tosatti, *Phys. Rev. B* 91, 045432-1 (2015).
55. A. Kumar and P.K. Ahluwalia, *Phys. B* 419, 66 (2013).
56. P.B. Johnson and R.W. Christy, *Phys. Rev. B* 6, 4370 (1972).
57. A.Y.-C. Yu and W.E. Spicer, *Phys. Rev.* 171, 834 (1968).
58. H. Pan and X.-S. Wang, *Nanoscale Res. Lett.* 10, 334 (2015).